Contents lists available at ScienceDirect

Electrochimica Acta

Improving electrochromic behavior of spray pyrolised WO$_3$ thin solid films by Mo doping

J.M. O-Rueda de León[a], D.R. Acosta[a,*], U. Pal[b], L. Castañeda[b]

[a] Instituto de Física, Universidad Nacional Autónoma de México, Apartado Postal 20-364, México, D.F. 01000, Mexico
[b] Instituto de Física, Benemérita Universidad Autónoma de Puebla, Apartado Postal J-48, Puebla, Pue. 72570, Mexico

ARTICLE INFO

ABSTRACT

The effects of molybdenum [Mo] doping on the electrochromic behavior of spray pyrolised tungsten trioxide [WO$_3$] thin films have been studied. It has been observed that the color-bleaching kinetics, coloration efficiency, and stability of electrochromic WO$_3$ films are closely related to molybdenum doping concentration, apart from their microstructure and crystallinity. While a nominal 6.0 at.% molybdenum doping produces best electrochromic response in WO$_3$ films, the electrochemical stability is highest when the nominal concentration of molybdenum is about 2.0 at.%. The improved electrochromic behavior of the Mo doped WO$_3$ films has been explained from the improved H$^+$ ion diffusion coefficient in the films during coloration and decoloration process.

1. Introduction

Electrochromic behaviors of tungsten trioxide [WO$_3$] thin films have been studied extensively for last 30 years due to their potential applications in display devices [1–5], rear view windows and "smart windows". The electrochromism is the process of changing transmittance and/or reflectance caused by an externally applied voltage, which is believed to occur through a reversible electron and cation intercalation, and for the case of WO$_3$ can be expressed as:

$$WO_3(transparent) + nM^+ + ne^- \Leftrightarrow M_nWO_3(blue) \qquad (1)$$
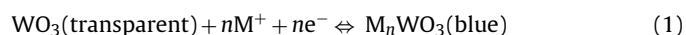
where M$^+$ is usually a hydrogen ion, or other cation like Li$^+$, Na$^+$. For most display applications, it is necessary that the formation of intercalated M$_n$WO$_3$ and its deintercalation/oxidation to form WO$_3$ occur very fast. While the rate of intercalation or coloration under applied electric field is controlled by the charge transfer at the WO$_3$–electrolyte interface, the bleaching or decoloration is controlled by the diffusion of proton in the WO$_3$. Therefore, the coloration kinetics of WO$_3$ thin films depend largely on their carrier concentration and mobility of the inserted ions, which indirectly depends on the texture, crystallinity, defect structures and impurity contents of the thin films.

A large variety of deposition techniques like thermal evaporation [6], sputtering [7], chemical vapor deposition [8], solution thermolysis [9], electrochemical [10], and spray pyrolisis [11–14] have been utilized to obtain WO$_3$ thin films with different morphologies, crystallinity and compositions. To enhance the electrochromic efficiency through transitions between two kinds of metal sites, efforts have also been made to fabricated thin films of selective mixed oxides semiconductors, based on their EC performance [15–17]. The electrochromic efficiency of WO$_3$ thin films can also be modified by doping suitable metal ions with higher electronegativity or lower oxidizing capability than W ions. Doping of such material in electrochromic host lattice is expected to benefit the coloration efficiency and durability of the host, extending the switching potential range, and enhancing the reaction kinetics. Bathe and Patil [18] have studied the influence of niobium [Nb] doping on the electrochromic properties of WO$_3$ thin films. It has been observed that though the incorporation of Nb up to 2.0 at.%

* Corresponding author at: Instituto de Física, Universidad Nacional Autónoma de México, Departamento de Materia Condensada, Ciudad Universitaria, 04510 Mexico, D.F., Mexico. Tel.: +52 55 5622 5117; fax: +52 55 5622 5011.
E-mail address: dacosta@fisica.unam.mx (D.R. Acosta).
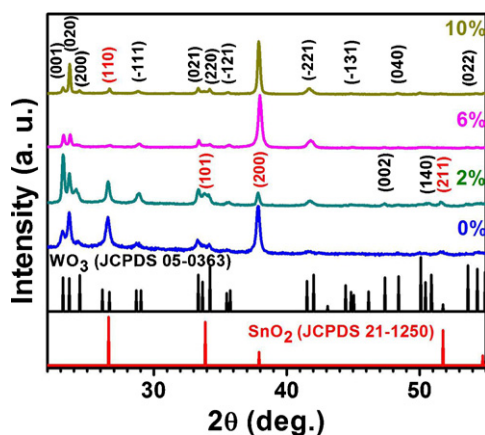
Fig. 1. XRD patterns of the undoped and Mo doped WO$_3$ thin films deposited over FTO coated glass substrates at 500 °C. The standard peak positions of WO$_3$ (JCPDS # 05-0363) and SnO$_2$ (JCPDS # 21-1250) are given at the bottom.

increases the charge capacity, reversibility and stability of the WO$_3$ thin films, their coloration efficiency decreases with the increase of Nb concentration. Though several elements like titanium [Ti], nickel [Ni], iron [Fe], vanadium [V], and molybdenum [Mo] have been tried to incorporate into WO$_3$ thin film matrix [19–21], considerable improvement of its electrochromic behavior has only been observed for Ti doping [22]. On the other hand, doped and undoped nanostructured WO$_3$ thin films have been efficiently utilized for photo-oxidation of water [23].

In the present work we report on the fabrication of nanostructured WO$_3$ thin solid films doped with different amounts of Mo by spray pyrolisis technique and their electrochromic behaviors. It has been demonstrated that the electrochromic characteristics like coloration efficiency, reversibility, and stability of WO$_3$ thin films can be improved by Mo doping in between 2.0 and 6.0 at.% (nominal).

2. Experimental details

2.1. Fabrication of molybdenum doped tungsten trioxide [WO$_3$:Mo] thin solid films

Spray pyrolisis technique was utilized to fabricate the doped and undoped WO$_3$ thin films. The WO$_3$ films were deposited on FTO/glass substrates utilizing a home-made device, based on the design reported by Castañeda et al. [24].

For depositing the FTO coatings over soda lime glass substrates, the same spray pyrolisis system was utilized. Ethanol ([C$_2$H$_5$OH], Sigma–Aldrich) solution (0.2 M) of tin(IV) chloride ([SnCl$_4$], Sigma–Aldrich), and aqueous solution of ammonium fluoride ([NH$_4$]F, Sigma–Aldrich) utilized as precursor solutions, were sprayed over soda lime glass substrates (2.54 cm × 2.54 cm) maintained at about 450 °C. The atomic ratio of fluorine and tin [F]/[Sn] in the precursor mixture was maintained 0.5. Estimated sheet resistances of the deposited FTO coatings were in between 7 and 10 Ω/square.

The molybdenum doped tungsten trioxide [WO$_3$:Mo] thin films were obtained from a starting solution containing tungsten(VI) chloride ([WCl$_6$], Sigma–Aldrich, 99.9%) dissolved in dimethylformamide ([HCON(CH$_3$)$_2$], Baker, 99.9%) with a molar concentration of 0.15 M. Molybdenum(VI) oxychloride ([MoO$_2$Cl$_2$], Alfa Aesar) was used as the dopant source. The nominal content of Mo in the thin films was varied from 2 to 10 at.% by adding different amounts of molybdenum(VI) oxychloride into the precursor solution. The final pH of the precursor solutions remained in between 4.0 and 5.0.

The soda lime glass substrates (2.54 cm × 2.54 cm) were ultrasonically cleaned with trichloroethylene ([C$_2$HCl$_3$], Baker), acetone ([CH$_3$COCH$_3$], Baker), methyl alcohol ([CH$_3$OH], Baker) sequentially, and dried under nitrogen flow. The substrates were then placed on a fused tin bath, maintained at 500 °C (±0.5 °C). The precursor solution was then sprayed over the substrates at the rate of 12 ml min^{-1} using filtered atmospheric air as carrier gas (8 l min^{-1}). The deposition was carried out for about 7.5 min.

2.2. Characterization of WO$_3$:Mo thin films

Thicknesses of the deposited thin films estimated using a surface profilometer (Tencor, model P15, resolution = 0.15 nm) varied in between 480 and 520 nm. Optical transmittance (T) spectra of the films were recorded through an Agilent HP 8453 UV–visible spectrometer, using an uncoated FTO/glass substrate as reference. Cu Kα$_1$ (λ = 1.5406 Å) radiation of an AXS D8 advanced X-ray diffractometer operating in the Bragg–Brentano geometry was used for recording the X-ray diffraction (XRD) patterns of the samples. A JEOL-5600 LV scanning electron microscope (SEM) attached with a Noran analytical system was used for morphological and composition evaluation of the thin films. A JEOL-100 CX, and a JEOL 2010-F field emission transmission electron microscope (TEM) were used for recording the low and high resolution TEM images of the samples, respectively. Electrochromic behaviors of the WO$_3$ and Mo doped WO$_3$ thin films were studied in a potentiostat/galvanostat (GillAC system) using a three electrodes electrochemical cell, using 0.001 M sulfuric acid ([H$_2$SO$_4$], Baker) solution (aqueous) as electrolyte. Platinum wires were used as pseudo reference and counter electrodes.

3. Results and discussion

3.1. Structural properties

X-ray diffraction patterns of the doped and undoped WO$_3$ thin films deposited on FTO/glass substrate are shown in Fig. 1. The diffraction patterns revealed several peaks related to WO$_3$ apart from the peaks arising from the FTO on the substrate. There appeared no diffraction peak related to molybdenum or its trioxide for the Mo doped WO$_3$ thin films. Intensity of the diffraction peaks associated to WO$_3$ increased with the increase of Mo concentration up to 8.0 at.% (nominal). However, for 10.0 at.% of Mo, the intensity of the diffraction peaks decreased. All the diffraction peaks could be indexed (Fig. 1) to the monoclinic phase of WO$_3$ (JCPDS # 05-0363). Appearance of sharp diffraction peak at about 2θ = 23.14° (d = 3.84 Å) for all the samples indicates a preferred orientation of the crystallites along the c-axis.

Average crystallite size of the thin films was estimated using the (2 0 0) peak of their XRD spectra using the Debye–Scherer formula [25]:

$$D = \frac{0.9\lambda}{B \cos \theta} \qquad (2)$$

where D is the crystallite size, λ is the wavelength of the incident radiation (Cu Kα line), θ is the Bragg angle and B is the FWHM of the diffraction peak measured in radians. Estimated crystallite size values for the doped and undoped thin films are listed in Table 1. As can be seen, the crystallite size of the WO$_3$:Mo thin films increases from 9.3 (±0.6) nm to 14.9 (±0.6) nm as the doping concentration in the solution increases from 0.0 to 10.0 at.%.

3.2. Scanning electron microscopy studies

Fig. 2 presents the typical SEM micrographs of the thin films doped with different concentrations of Mo. Formation of films with
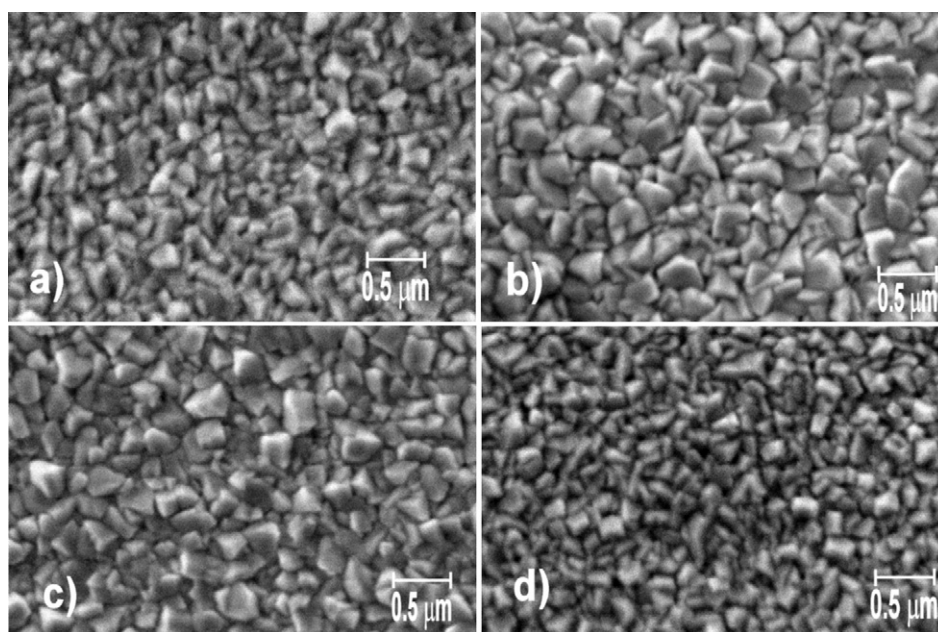
Fig. 2. Typical SEM images of the: (a) undoped, (b) 2.0 at.% Mo, (c) 6.0 at.% Mo, and (d) 10.0 at.% Mo doped WO$_3$ thin solid films prepared by spray pyrolisis.

nanometer particles with sizes running from 80 to 350 nm is clear from the micrographs. All the films look regular, dense and compact without void or inter grains spacing. Most of the particles in the samples are well faceted crystallites. On incorporating Mo at nominal 2.0 and 6.0 at.%, the size of the crystalline grains increased. However, incorporation of Mo at 10.0 at.% produced smoother thin films with relatively smaller grain size. Therefore, the amount of Mo in the starting solution affects the grain growth and hence the morphology of the film surface. Energy dispersive spectroscopy (EDS) analysis revealed that the concentrations of incorporated Mo in the samples (Table 1) were much lower than their nominal concentrations.

3.3. Transmission electron microscopic studies

Fig. 3(a–d) displays high resolution transmission electron microscopy (HRTEM) images from pure and Mo doped WO$_3$ thin films. For each Mo concentration, the left hand images correspond to as-obtained HRTEM micrographs. The inverse fast Fourier transform micrographs and the crystallographic analysis processed using the Digital Micrograph software results are presented at the middle and right columns respectively. The HRTEM images revealed that all the samples consist of crystalline grains with quite defined lattice planes. The inter-planer distance d between the most frequently occurring lattice planes was estimated to be 0.376 nm. Even though in lesser frequencies, several other planes

were also revealed in the HRTEM images of the samples, indicating their polycrystalline nature. FFTs of the selected area HTEM images of the samples revealed that most of the lattice planes are aligned perpendicular to the [1 1 0] zone axis. The lattice planes [(0 0 1), (2 0 0), (0 2 0), (0 2 1), (0 2 2), and (2 2 1)] revealed in the FFTs, correspond well with the diffraction planes revealed in the XRD patterns of the samples.

3.4. Optical properties

Fig. 4 shows the optical transmittance spectra of the films in 300–850 nm spectral range at bleached condition. The film containing 2 at.% of Mo revealed higher transmittance than the other samples (inset, Fig. 4). On increasing the Mo concentration further, the film transmittance decreased, as has been seen by Gesheva et al. [26]. Absorption coefficients at different wavelengths were calculated from the transmittance spectra using the relation:

$$\alpha = \frac{1}{\delta} \ln(1/T) \tag{3}$$

where δ was the thickness of the film. The absorption coefficient of a direct band gap semiconductor like WO$_3$ follows the relation [27]:

$$\alpha = k \frac{(h\nu - E_g)^{n/2}}{h\nu} \tag{4}$$

Table 1
EDS composition and average crystallite size values in the WO$_3$ films doped with different Mo concentrations.

Nominal dopant concentration (at.%)	Crystallite size (nm) ± 0.5 nm	EDS composition (at.%)		
		W	O	Mo
0	09.3	23.5	76.5	0.0
2	07.5	19.2	80.4	0.4
6	12.2	21.7	77.7	0.6
10	14.9	19.2	79.9	0.9
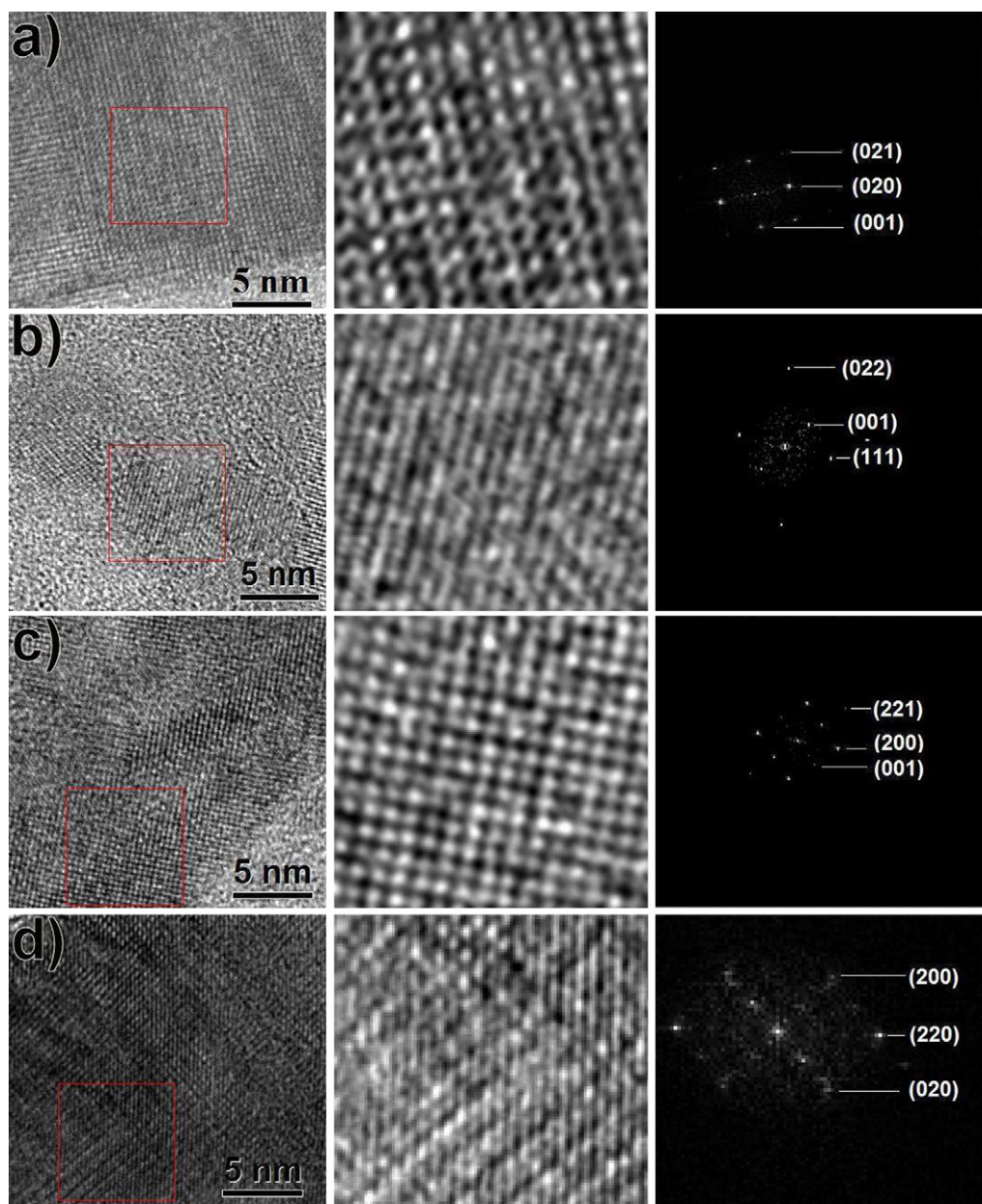
Fig. 3. Typical high resolution TEM micrographs of the: (a) undoped, (b) 2.0 at.% Mo, (c) 6.0 at.% Mo, and (d) 10.0 at.% Mo doped WO_3 thin films. Amplified images of the corresponding selected area and their FFTs are presented in the middle and right columns, respectively.

where k is a constant, E_g is the band gap energy of the semiconductor, and n is a constant, equal to 1 for direct transition. The band gap energy values for the doped and undoped films were estimated from the $(ah\nu)^2$ vs. photon energy $(h\nu)$ plots as shown in Fig. 4. The band gap energy of the samples varied from 3.38 to 3.49 eV. As has been reported by Deb [28], the band gap energy of WO_3 films can vary from 3.27 to 3.65 eV depending on their crystallinity. As has been observed from the XRD patterns of our WO_3 thin films (Fig. 1), they are polycrystalline in nature. On 2.0 at.% Mo doping, the band gap of the films increased to about 3.49 eV (±0.06 eV). On increasing the Mo concentration further, the band gap energy of the films decreased and finally reached to the band gap energy value of the undoped film (3.38 $\pm$ 0.05 eV) for 10 at.% Mo doping. Patil and Patil [29] have a band gap value of 2.76 eV for their spray pyrolised MoO_3–WO_3 thin films. On the other hand, Ivanova et al. [17] have reported the band gap energy of about 3.23 eV for similar films deposited by CVD technique.

3.5. Cyclic voltammetry (C–V)

As has been mentioned in the experimental section, the electrochemical behavior of the thin film samples was studied in an electrochemical shell with three electrode arrangement. In the cell, the metal oxide thin film served as working electrode and two platinum wires were used as standard and counter electrodes. During the potential sweep, the current resulting from ion intercalation and deintercalation is measured. The potential sweep was performed in between −800 mV and +1200 mV. Depending on the dopant concentration and number of cycles, a cathodic scan below −800 mV caused the films to turn blue, and an anodic scan above −550 mV resulting them to turn transparent. It has been observed that the intercalation and deintercalation process in the films occur at different potentials depending on the Mo concentration in them. The cyclovoltammertic curves show distinct cathodic and anodic peaks as a result of insertion and extraction of H^+ ions in/out the
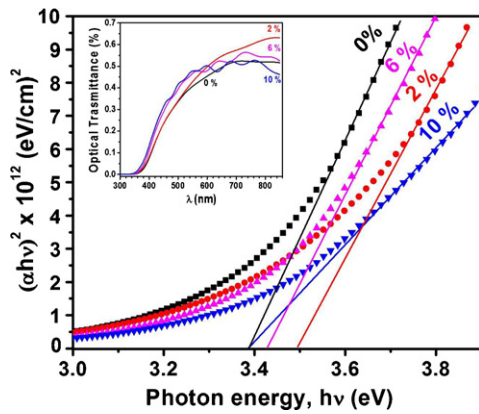
Fig. 4. The $(ah\nu)^2$ vs. $h\nu$ plots derived from the optical transmittance spectra (inset) of the Mo doped and undoped WO_3 thin films. Variation of optical band gap on Mo doping is clear from the linear extrapolations of the $(ah\nu)^2$ vs. $h\nu$ plots to the energy axis.

film structure. On the other hand, the coloration and decoloration potentials for a particular film vary from cycle to cycle. As can be seen from Fig. 5, on increasing the Mo concentration in the films, while the cathodic/insertion peak moves to higher potential, the anodic/extraction peak moves to a lower potential, which indicates that the changes from colored to bleach state and vice versa are faster for the WO_3 films doped with Mo. The bleaching reversibility of all the films was good up to 1000th cycles at 2.0 at.% of Mo in WO_3 films. Increasing substantially the cycles (2000th cycles) the current–voltage curve is flatted (see Fig. 5a) and it become difficult to distinguish between simple charge transfer. Indeed, the shape of the cyclic voltammetric curves depends strongly on

the values the kinetic parameters of the system. When the Mo concentration increased to 6.0 at.%, the coloration and bleaching transition of the WO_3 films increased with respect to 2.0 at.%. This effect is related with the ion intercalation and deintercalation transport. However, we have observed a current anomaly at 1000th cycles, i.e., the current value increased four times with respect to another cycles, see Fig. 5b. At 10.0 at.% of nominal Mo concentration, the cyclic voltammograms have the same behavior as that of 2.0 at.%, except that the flatted current–voltage curve was found at 1000th cycles (see Fig. 5c). In Tables 2–4, the electrochemical parameters such as cathodic peak voltage (V_{pc}), anodic peak voltage (V_{pa}), maximum cathodic current (i_c), maximum anodic current (i_a) and the coefficient effective diffusion. For the doped and undoped samples at different cycles of cyclic voltammograms are presented.

The coloration and bleaching processes of WO_3 films are associated with the intercalation (insertion) and deintercalation (extraction) of H^+ ions and electrons, which depend on the mobility of H^+ ions in the films. The mobility of the H^+ ions in the film also depends strongly on the density of the film; its degree of porosity, and surface characteristics. To estimate the mobility of H^+ ions in our thin films, its diffusion coefficients into the Mo doped and undoped WO_3 films are estimated using the Randle–Sevcik equation [30]:

$$i_p = 2.72 \times 10^5 \, n^{3/2} \, D^{1/2} \, Co \, \nu^{1/2} \tag{5}$$

where D is the diffusion coefficient, Co is the concentration of active ions in the electrolyte solution, ν is the scan rate, n is the number of electrons transferred in the redox event which is assumed to be 1, i is the peak current density (i_a, anodic peak current density; i_c, cathodic peak current density). By substituting all the values, for the used scan rate of 60 mV/s, the diffusion coeffi-
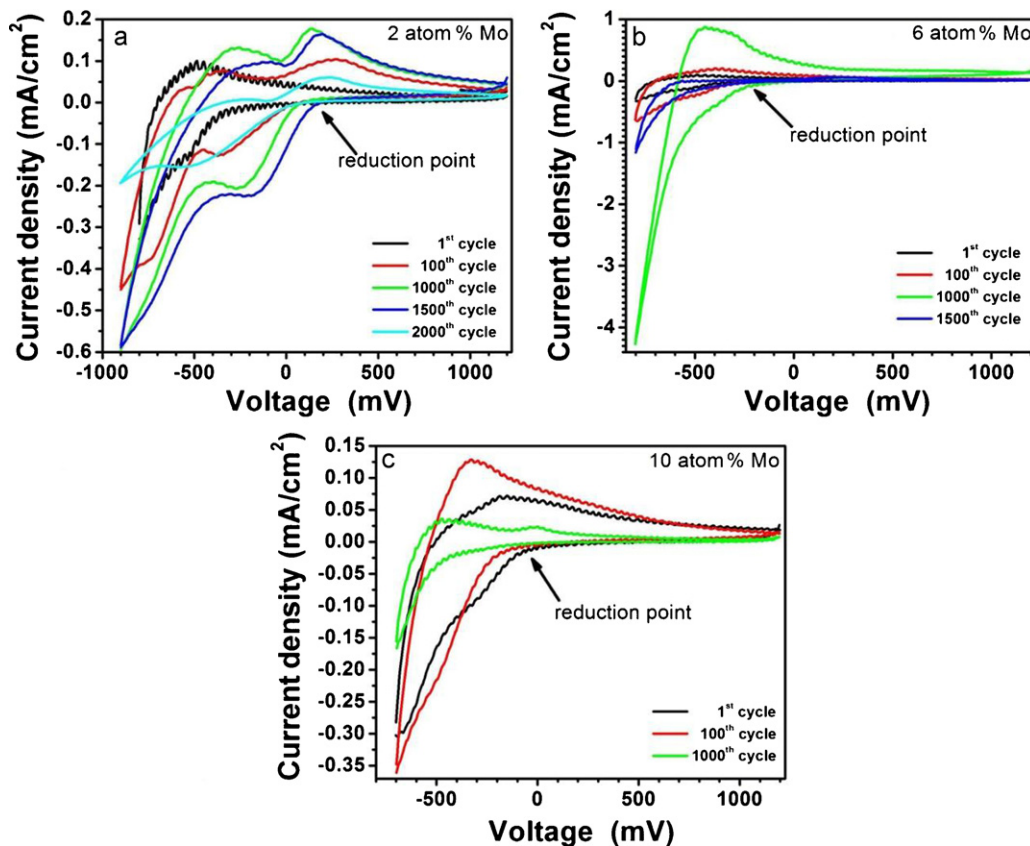
Fig. 5. Voltammograms of the undoped, 2.0 at.% Mo doped, 6.0 at.% Mo doped, and 10.0 at.% Mo doped WO_3 thin films at different voltammetric cycles. Observed reduction points for the samples are shown by arrows.
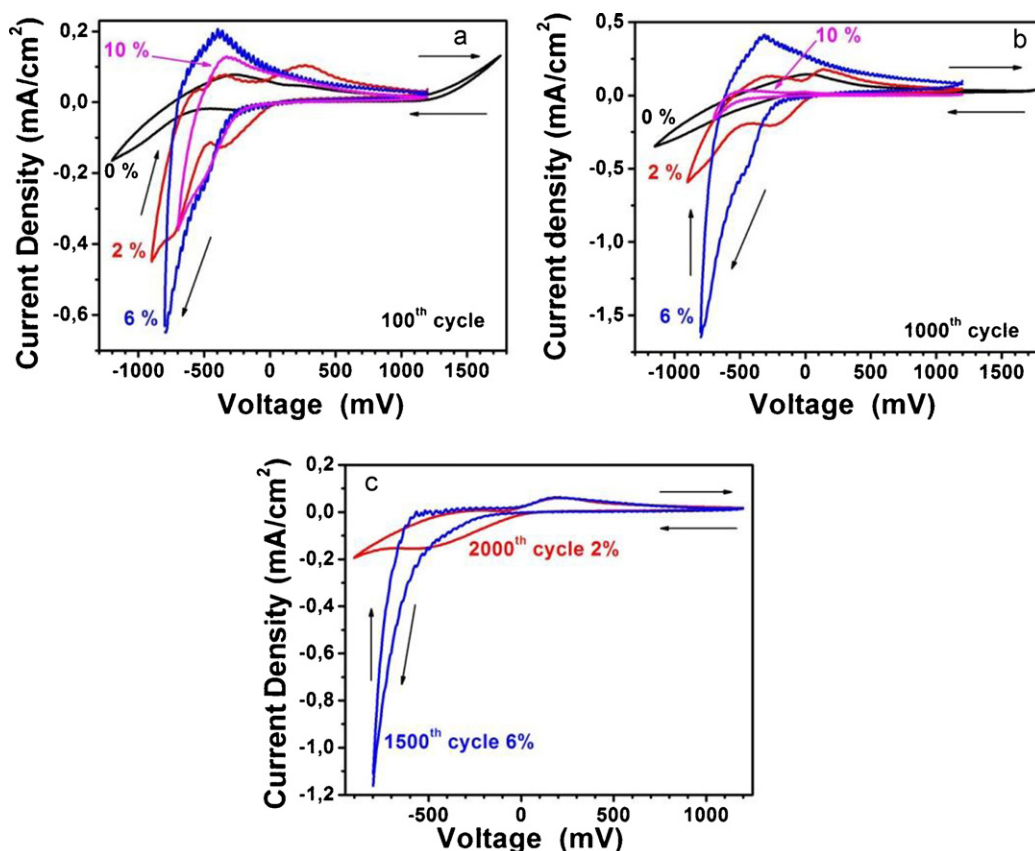
Fig. 6. Comparative voltammograms of the Mo doped and undoped WO$_3$ samples at their (a) 100th, (b) 1000th, and (c) 2000th voltammetric cycles.

Table 2
Electrochemical parameters and H$^+$ ion diffusion coefficients in the undoped and Mo doped WO$_3$ thin films evaluated at their 100th voltammetric cycle.

Nominal doping Mo (at.%)	V_{pc} (mV)	i_c (mA)	D_{insert} (cm^2 s^{-1}) $\pm$ 10%	V_{pa} (mV)	i_a (mA)	$D_{extract}$ (cm^2 s^{-1}) $\pm$ 10%
0	−1200	−0.1647	4.07×10^{-12}	265.6	0.0779	9.11×10^{-13}
2	−900	−0.4440	2.96×10^{-11}	−345.2	0.0774	8.99×10^{-13}
6	−800	−0.6479	6.30×10^{-11}	−394.3	0.2069	6.43×10^{-12}
10	−700	−0.3612	1.96×10^{-11}	−328.5	0.1286	2.48×10^{-12}

V_{pc} = cathodic peak voltage; i_c = cathodic peak current; D_{insert} = insertion diffusion coefficient calculated from C–V; V_{pa} = anodic peak voltage; i_a = anodic peak current; $D_{extract}$ = extraction diffusion coefficient calculated from C–V.

Table 3
Electrochemical parameters and H$^+$ ion diffusion coefficients in the undoped and Mo doped WO$_3$ thin films evaluated at their 1000th voltammetric cycle.

Nominal doping Mo (at.%)	V_{pc} (mV)	i_c (mA)	D_{insert} (cm^2 s^{-1}) $\pm$ 10%	V_{pa} (mV)	i_a (mA)	$D_{extract}$ (cm^2 s^{-1}) $\pm$ 10%
0	−1200	−0.3489	1.82×10^{-11}	17.7	0.1446	3.14×10^{-12}
2	−900	−0.5935	5.29×10^{-11}	−261.2	0.1321	2.62×10^{-12}
6	−800	−1.6479	4.08×10^{-10}	−314.1	0.4143	2.58×10^{-11}
10	−700	−0.1662	4.15×10^{-11}	−474.7	0.0356	1.90×10^{-13}

V_{pc} = cathodic peak voltage; i_c = cathodic peak current; D_{insert} = insertion diffusion coefficient calculated from C–V; V_{pa} = anodic peak voltage; i_a = anodic peak current; $D_{extract}$ = extraction diffusion coefficient calculated from C–V.

Table 4
Electrochemical parameters and H^+ ion diffusion coefficients in the undoped and Mo doped WO$_3$ thin films evaluated at their 2000th voltammetric cycle.

Nominal doping Mo (at.%)	V_{pc} (mV)	i_c (mA)	D_{insert} (cm^2 s^{-1}) $\pm$ 10%	V_{pa} (mV)	i_a (mA)	$D_{extract}$ (cm^2 s^{-1}) $\pm$ 10%
0	–	–	–	–	–	–
2	−900	0.1941	5.66×10^{-12}	−234.7	0.0603	5.46×10^{-13}
6	−800	1.1098	1.85×10^{-10}	−550.9	0.0148	3.29×10^{-14}
10	–	–	–	–	–	–

CV$_{pc}$ = cathodic peak voltage; i_c = cathodic peak current; D_{insert} = insertion diffusion coefficient calculated from C–V; V_{pa} = anodic peak voltage; i_a = anodic peak current; $D_{extract}$ = extraction diffusion coefficient calculated from C–V.

cient of H$^+$ ions during insertion (D_{insert}) and extraction (D_{extract}) were calculated (Tables 2–4), which, for our undoped WO$_3$ films were 4.07×10^{-12} cm^2/s and 9.11×10^{-13} cm^2/s, respectively. In general, these values for WO$_3$ thin films estimated through different techniques are found to vary in between 1×10^{-10} cm^2/s and 2×10^{-12} cm^2/s [31,32]. The diffusion coefficient values estimated for our undoped WO$_3$ films are in agreement with values reported by Batchelor et al. [32] and Randin et al. [33]. The diffusion coefficient values obtained for our Mo doped WO$_3$ films were also in agreement with the values reported by Patil et al. [9]. From Tables 2–4, we can observe that both the insertion diffusion coefficient (D_{insert}) and extraction diffusion coefficient (D_{extract}) of H$^+$ ions in our WO$_3$ films increased with Mo doping. However, this trend changed when the voltammetric cycle reaches close to the break-down point of the film. Comparative response of the Mo doped and undoped WO$_3$ films at their 100th, 1000th, and 2000th voltammetric cycles are presented in Fig. 6. As can be seen from the figure, the WO$_3$ film doped with 6.0 at.% of Mo presents best electrochromic response, while the film doped with 2.0 at.% manifests best electrochemical stability. Therefore, WO$_3$ thin films nominally doped with Mo in the range of 2.0–6.0 at.% are suitable for electrochromic applications. As can be seen from Fig. 5, even for the same scan rate, the cathodic current varied from scan-to-scan for a particular sample, indicating structural change in the analyte due to redox reaction, probably changing its stoichiometry during the electrochemical process. The effect of sample stoichiometry on the cathodic current and redox current could also be perceived from Tables 2 and 3 where, for a particular scan, the cathodic current varied with the variation of nominal Mo content in the samples. Finally, its worth to mention that the Randles–Servcik equation used for the estimation of diffusion coefficient of H$^+$ ions in our doped and undoped WO$_3$ samples are better suited for the reversible current–voltage characteristics. On the other hand, chromoamperometry or chronocolumnometry technique would have given more precise values of H$^+$ ion diffusion coefficient in the present case [34,35]. However, the cyclic voltammetric technique used in the present work for the static condition (no liquid flow) visualized more clearly the degradation kinetics of our thin film samples which is very important for their practical applications.

4. Conclusions

In summary, we could fabricate compact nanocrystalline WO$_3$ thin films with different concentrations of Mo doping by spray pyrolisis process. Incorporation of Mo in WO$_3$ thin films modifies their crystallinity, crystallite size, and optical band gap. Electrochomatic performance of the spray pyrolised WO$_3$ thin films improves significantly on Mo doping. While the best electrochromic response of WO$_3$ thin films could be obtained through Mo doping of about 6.0 at.%, stability of the films is best when the nominal dopant concentration is about 2.0 at.%. Spectroscopic nonlinear optical analyses on these materials are currently in progress to explore their applications in other optical applications like in photonics.

References

[1] D. Davazoglu, A. Donnadieu, Thin Solid Films 164 (1988) 369.
[2] B.W. Faughnan, R.S. Crandall, Display devices, in: J.L. Pankov (Ed.), Topics in Applied Physics, Springer Verlag, Berlin, 1980, p. 113.
[3] H.S. Witham, P. Chindaudom, I. An, R.W. Collins, R. Messier, K. Vedam, J. Vac. Sci. Technol. A 11 (4) (1993) 1881.
[4] C.G. Granqvist, Handbook of Inorganic Electrochromic Materials, Elsevier, Amsterdam, 1995, p. 17.
[5] C.G. Granqvist, M.H. Francombe, J.L. Vossen (Eds.), Physics of Thin Films: Mechanic and Dielectric Properties, vol. 17, Academic Press, Inc, San Diego, 1993, p. 307.
[6] J.P. Randin, R. Viennet, J. Electrochem. Soc. 129 (10) (1982) 2349.
[7] R.A. Batchelor, M.S. Burdis, J.R. Siddle, J. Electrochem. Soc. 143 (3) (1996) 1050.
[8] O. Bohnke, C. Bohnke, A. Donnadieu, D. Davazoglou, J. Appl. Electrochem. 18 (1988) 447.
[9] P.R. Patil, S.H. Pawar, P.S. Patil, Solid State Ionics 136–137 (2000) 505.
[10] M. Rezrazi, B. Vuillemin, O. Bohnke, J. Electrochem. Soc. 138 (1991) 2770.
[11] P.S. Patil, S.B. Nikam, L.D. Kadam, Mater. Chem. Phys. 69 (2001) 77.
[12] R. Sivakumar, A.M.E. Raj, B. Subramanian, M. Jayachandran, D.C. Trivedi, C. Sanjeeviraja, Mater. Res. Bull. 39 (2004) 1479.
[13] J.M. Ortega, A.I. Martinez, D.R. Acosta, C.R. Magaña, Sol. Energy Mater. Sol. Cells 90 (2006) 2471.
[14] S.R. Bathe, P.S. Patil, Sol. Energy Mater. Sol. Cells 91 (2007) 1097.
[15] T. Ivanova, K. Gesheva, A. Szekeres, J. Solid State Electrochem. 7 (2002) 21.
[16] P.S. Patil, S.H. Mujawar, A.I. Inamdar, S.B. Sadale, Appl. Surf. Sci. 250 (2005) 117.
[17] T. Ivanova, K.A. Gesheva, G. Popkirov, M. Ganchev, E. Tzvetkova, Mater. Sci. Eng. B 119 (2005) 232.
[18] S.R. Bathe, P.S. Patil, J. Phys. D: Appl. Phys. 40 (2007) 7423.
[19] A. Donnadieu, in: C.M. Lampert, C.G. Granqvist (Eds.), Large-Area Chromogenics: Materials and Devices for Transmittance Control, vol. IS4, SPIE Opt. Eng. Press, Bellingham, 1990, p. 191.
[20] T. Yoshimura, J. Appl. Phys. 57 (1985) 911.
[21] R. Azimirad, O. Akhavan, A.Z. Moshfegh, Thin Solid Films 484 (2005) 124.
[22] S. Hashimoto, H. Matsuoka, J. Electrochem. Soc. 138 (1991) 2403.
[23] H. Wang, T. Lindgren, J. He, A. Hagfeldt, S.-E. Lindquist, J. Phys. Chem. B 104 (2000) 5686.
[24] L. Castañeda, R. Silva-González, J.M. Gracia-Jiménez, M.E. Hernández-Torres, M. Avendaño-Alejo, M. César Márquez-Beltrán, L. de la Olvera, J. Vega-Pérez, A. Maldonado, Mater. Sci. Semicond. Process. 13 (2010) 80.
[25] B.E. Warren, X-Ray Diffraction, Dover, New York, USA, 1990, p. 253.
[26] K.A. Gesheva, A. Cziraki, T. Ivanova, A. Szekeres, Thin Solid Films 515 (2007) 4609.
[27] T.S. Moss, Optical Properties of Semiconductors, Butterworth, London, 1961, p. 14.
[28] S.K. Deb, Philos. Mag. 27 (1973) 801.
[29] P.R. Patil, P.S. Patil, Thin Solid Films 382 (2001) 13.
[30] R.S. Nicholson, I. Shain, Anal. Chem. 36 (1964) 706.
[31] E. Burstein, Phys. Rev. 93 (1954) 632.
[32] R.A. Batchelor, M.S. Burdis, J.R. Siddle, J. Electrochem. Soc. 143 (1996) 1050.
[33] J.P. Randin, R. Viennet, J. Electrochem. Soc. 129 (1982) 2349.
[34] A. Lasia, Can. J. Chem. 64 (1986) 2319.
[35] P.J. Kuleza, L.R. Faulkner, J. Am. Chem. Soc. 110 (1988) 4905.